CuO and MWCNTs Nanoparticles Filled PVA–PVP Nanocomposites: Morphological, Optical, Thermal, Dielectric, and Electrical Characteristics

Hassan A. H. Alzahrani[1]

Abstract

Copper dioxide (CuO) nanoparticles and Multiwall carbon nanotubes (MWCNTs) filled poly(vinyl alcohol) (PVA) and poly(vinyl pyrrolidone) (PVP) blend matrix (50/50 wt%) based polymer nanocomposites (PNCs) (i.e., PVA/PVP:(15-x) CuO(x)MWCNTs for x = 0,1,5,7.5, 10,14, and 15wt%) have been prepared employing the solution-cast method. The morphologies of these PNCs are semicrystalline, according to an X-ray diffraction investigation. The FTIR, SEM, and AFM measurements of PNCs were used to investigate the development of the miscible mix, polymer-polymer and polymer–nanoparticle interactions, and the influence of CuO and MWCNTs nanofillers on the morphology aspects on the main chain of PVA/PVP blend. The nanofiller dispersion signposting for x = 14 wt% nanoloading in the PVA–PVP blend matrix significantly enhances the crystalline phase, diminishing the optical energy gap to 2.31 eV. The DC conductivity values augment with the upsurge in nanofiller level for maximum x = 14 wt%. The dielectric and electrical characteristics of these PNCs are investigated for an applied frequency range from 1 kHz to 1 MHz. The enhancement in the nanofiller level upto x = 14 wt% in the PVA/PVP matrix leads to the development of percolating network through the PNCs. These factors boost the dielectric permittivity values substantially, owing to the decrease in the nano-confinement phenomenon. The rise in applied frequency reduces dielectric permittivity and impedance values and enhances ac electrical conductivity. These PNCs having good dielectric and electrical characteristics can be used as frequency tunable nanodielectric material in electronic devices.

1 Introduction

Nowadays, engineering polymers have become a part of polymers, which are persistently suitable for high temperatures with strong structural, optical and electronic properties, excellent geometrical durability, strong weather resilience, and fatigue strength [1–4]. In this regard, polymer mixing, or a blend of polymers, is a class of engineering polymers identical to metallic ingots obtained by combining a minimum of two polymers to produce a distinct substance with varied fundamental characteristics [5, 6]. The creation of polymer blends involves many distinct procedures such as melting, solution blending, latex melding, partial blocking or grafting copolymerisation and developing interpenetrating polymeric networks [7, 8]. Out of these procedures, as mentioned above the solvent blending is a highly economical and simplest way of production of polymer blends. The procedure includes the mixing of two or more polymers that are frequently immiscible and have compatible components. The compatibility should increase the regularity of the microstructures and the functionality of that substance regarding structural and bonding characteristics. The poly(vinyl alcohol) (PVA) and poly(vinyl pyrrolidone) (PVP) mixture have developed remarkable qualities in this respect, having excellent characteristics such as high elasticity, flexibility, non-toxicity, good mechanical strength and are thermally stable materials. [9–11]. The additional benefits of these combinations include water-soluble, miscible, excellent electro-optic properties and composite materialising characteristics [12, 13]. Many researchers are involved in their innovative investigation using PVA–PVP mixtures filled with nanoparticles to

✉ Hassan A. H. Alzahrani
hahalzahrani@uj.edu.sa

1 Department of Chemistry, College of Science and Arts at Khulis, University of Jeddah, P.O. Box 355, Jeddah, Saudi Arabia

create a new polymer blend nanocomposite (PNCs) for any appropriate device applications [2, 14]. Out of many fillers, nanoparticles to be incorporated in the polymer matrix, the copper oxide (CuO), and multiwall carbon nanotubes (MWCNTs) have emerged as excellent nanofillers due to versatile applications in present-day technology [15, 16]. The CuO nanoparticles belong to a class of transition metal oxide, with monoclinic structures and p-type semiconducting properties. These highly stable CuO nanofillers also have fascinating features such as exceptional thermophysical abilities, good dispersion ability, photovoltaic capabilities, and antibacterial activity [17]. On the other hand, other nanofiller multiwall carbon nanotubes (MWCNTs) contain many popped graphene sheets comprising structural complexity and variation. Conversely, MWNTs benefit from massive manufacturing facilities, the cheap unit expense of production, improved thermodynamic features, and chemically resilient materials. These MWCNTs are applicable in sensitive gas detection materials, dielectric and technologically challenging applications, such as field-emission and optoelectronic screens [18]. In this current research, we have developed PVA–PVP:(15-x)CuO(x) MWCNTs nanocomposite by utilizing solvent casting method for various filler level x = 0, 1, 5, 7.5, 10, 14, 15 wt%. The solvent casting method's advantages involve obtaining uniform thickness, better gloss, flexibility, economical, and no defects (die lines, extrusion, etc.) composites. The prepared PVA–PVP:(15-x)CuO(x) MWCNTs PNCs are further used to explore its structural, optical, dielectric and electronic properties for any possible device applications.

2 Materials and Methods

2.1 CuO Nanoparticles

Throughout the research work, only essential laboratory solution grades were employed to synthesise CuO nanofillers. The reagents (Cu $(C_2H_3O_2)_2$) and NaOH used during this current study are procured by Sigma Aldrich, Germany. Eventually, 0.02 mol of liquid copper acetate mixture is prepared by adding 1 ml glacial acetic acid and boiled at 110 °C at a continuous mixing rate of 500 rpm for 1 h using a temperature-controlled mechanical agitator. Subsequently, 1 M NaOH acid is transferred to the sample described above solutions such that a dark cloud is generated. The precipitation induced throughout the combination is extracted to create copper oxide nanofillers using a centrifuge. This CuO aggregate is repeatedly rinsed using deionising water until all NaOH residues with neutrality pH values are eliminated. The obtained CuO was subsequently dried for eight hours to eliminate the humidity component at 500 °C in an oven, and the estimated yield was about 94%. XRD and SEM were evaluated to explore the crystallographic phase formation of CuO powder.

2.2 Preparation of Carboxylated MWCNTs

Carbon nanotubes are externally modified to introduce unique characteristics such as increased functionality dispersal, compatibility, or reduced toxic effects. Thus, 75 mg of Multi-walled carbon nanotubes (MWCNTs with 3.5 nm diameter, 1–10 μm length having purity > 90% and specific surface area >500 m^2/g) was purchased through Sigma Aldrich, Germany and dipped in hydrochloric acid (HCl) for 24 h. These drenched MWCNTs in HCl solution is mixed with 500 ml of distilled water and swirled using a vigorous stirring rate of 500 rpm approximately for 20 min. The stirred mixture was further filtered utilising pore 0.1 μm Whatman Nylon filter membrane. The acquired remnant mixture is repeatedly treated thoroughly till the pH level of the filtrated mixture becomes neutral. Subsequently, produced MWCNTs were dried in the vacuum oven maintained at 600^0 C for 20 h to eliminate the water component. Finely, altered MWCNTs were disseminated in sulfuric acid (H_2SO_4) and nitric acid (HNO_3) combination obtained in 3:1 volume proportion and homogenised by utilising probe ultrasonicator (PCI Analytics, India) for 2 h. The dispersed mixture is rinsed with distilled water until the filtrated solution is neutral and then screened using a 0.1 μm Whatman Nylon filter membrane. The precursor is heated in a vacuum oven, and the quantity of the carboxylated MWCNTs generated (MWCNT-COOH) is 73.2 mg.

2.3 PVA/PVP Polymer Nanocomposites

8 g of Mowiol 4-88 of (PVA of Sigma Aldrich Germany, average molecular weight ~31000) are mixed into 80ml deionised water and agitated for an hour at 90 °C temperature to produce a clear liquid. Likewise, 80ml deionised water was mixed to 8 g of Poly vinyl pyrrolidone (PVP, average molecular weight~40000, Sigma Aldrich Germany). This combination is agitated at 70 °C and 500 rpm for two hours to produce a suitable liquid. The clear, viscous liquid was again mixed (at 300 rpm) for 1 h at room temperature employing a mechanical stirrer. The dense mixture formed is partitioned into eight equal portions. This PVA–PVP :(15-x) CuO(x) MWCNTs nanocomposites of various 'x' nanofiller loading are produced by the subsequent equation,

$$x\% = \frac{W_d}{(W_d + W_p)} \times 100 \qquad (1)$$

where W_d is the weight of the added nanofillers and W_p is the weight of the host polymer blend.

Synthesised ZnO and MWCNTs nanofillers have been introduced with a weight of x = 0, 1, 5, 7.5, 10, 14 and 15. Furthermore, fill the nanofillers on every area of the PVA/PVP mix employing ultrasonicator for 10 min, unless every nanofillers are uniformly dispersed. Each part of PVA–PVP:(15-x)CuO(x)MWCNTs solution is placed on a glass petri plate and stored in a furnace set at 50 °C for drying tonight. Every nano-composites film is stripped and enveloped inside a silver sheet and stored inside a vacuum chamber for additional analysis.

2.4 Measurements

The overall thickness of PVA–PVP:(15 − x)CuO(x)MWC-NTs PNCs were estimated 165–180 μm employing a DektaK stylus profilometer (Bruker). The structural parameters of PVA–PVP:(x)CuO(15-x) MWCNTs for different nanofiller loading are detected by the Empyrean third-generation Malvern Panalytical X-ray Diffractometer in the Cu-Ka reflections (μ?=?1,5406 A). Using KBr Pellets Varian Excalibur FTIR Spectrometer in the 500 to 4000 cm^{-1} range, the FTIR spectra of PNCs are acquired with 50 scans and 2 cm^{-1} precision. SEM EVO 18 ALTO 1000 cryo-scanning model is employed to study the morphological structure, particle size estimate, and content of PVA–PVP:(15-x)CuO(x)MWCNTs nanocomposites. The surface roughness and morphological developments were obtained utilizing the solver-PRO (NT-MDT) AFM instrument. In an environmental chamber at heating intervals of 10 °C/min, the heat degradation was studied in a range of temperatures from 35 to 650 °C adopting a Shimadzu Thermogravimetric-45 H. The visible spectrometer Shimadzu UV is used to assess the optical properties such as energy gap. The dielectric loss tangent of PVA–PVP:(15-x)CuO(x)MWCNTs for real and complicated dielectric nanocomposites is evaluated employing the 4200-SCS Keithley parameter analyser at rooms from 1 kHz to 1 MHz across frequency bands. PL spectra were produced from a photoluminescent spectrum by fluorescence spectrophotometer-Cary eclipse (Varian) by utilising emission and arousal slit size 5 nm, scanning rate 120 nm/min,

data interval 1 nm (average time 0.5 s), PMT voltage 600 V, and exc = 325 nm wavelength by excitation.

3 Results and Discussions

3.1 XRD Spectra

Figure 1 illustrates the XRD spectra of PVA–PVP:(15-x) CuO(x)MWCNTs at loading levels of the 'x' filled compound, x ranging from 0, 1, 5, 7.5, 10, 14, and 15 wt%. Filled MWCNTs exemplify a slight bump in the MWCNTs' diffraction angle at 26.52° (JCPDS file no: 48-1449) [19]. On the other hand, peaks arise at 2θ = 21.6º, 29.7º, 36.5º, 42.4º, and 61.4º, analogous to (014), (110), (111), (200), and (‾113) orientation signpost the presence of CuO nanoparticles [20]. A comprehensive, substantial rise at scattering angle 19°< 2θ<?20° can be seen, which suggests the existence of the semicrystalline peak of PVA (more precisely, of polyvinyl acetate). The peak witnessed at 21.21°, corresponding to d-values of 4.1544 Ǔ indicates the PVP polymer long chain [20]. The breadth of semicrystalline peaks of PVA–PVP nanocomposite varies due to incorporating nanofillers, which reveals an increase in the crystalline parameters. The strength of the crystallised spikes of PVA–PVP rises in tandem with the filler level, and the findings are most pronounced for the filler level x = 14%. Enhancing complex conformation involves the OH group of PVA–PVP backbone sequence and CuO/MWCNT nanofillers, which leads to gain in the crystalline phase. Thus, PVA–PVP peaks move onto the lesser angle with the upsurge in filler level.

Table 1 further depicts the microstructural strain (also known as strain), dislocation density (also known as density), and crystallinity (also known as phase) of each PVA–PVP: (15-x)CuO(x)MWCNTs for various filler loading. The crystallite size in polymer nanocomposite measures the molecular disorder by implanting nanoparticles in the PVA–PVP polymer's backbone. We have developed an algorithm using PowderX software (http://powdex.eng.umich.edu) to enunciate the crystallinity behaviour of composite

Table 1 Crystalline values of PVA–PVP/(15-x)CuO(x) MWCNTs

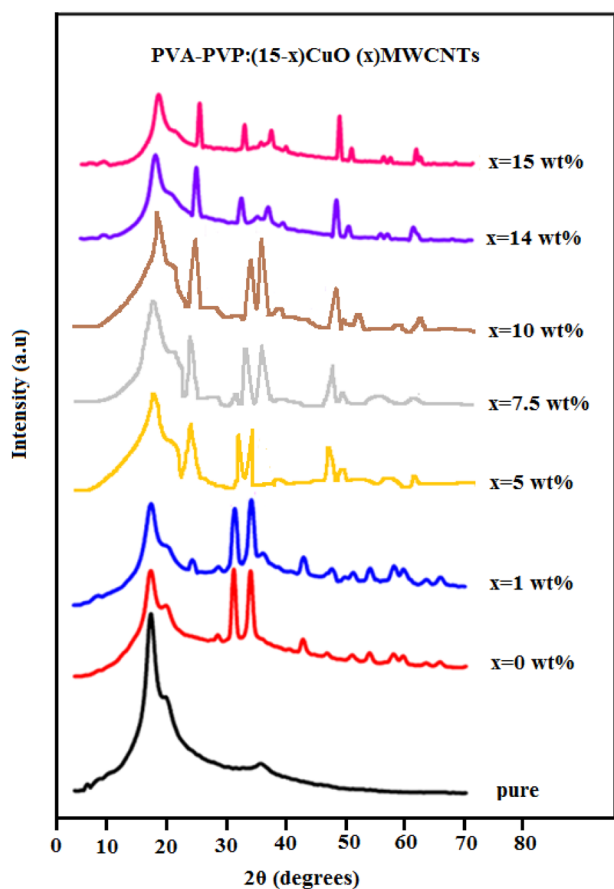| Dopants concentrations	% Crystallinity	D (nm)	Microstrain (e) x 10^{-3}	d (10^{16} lines/m^2)
Pure PVA–PVP	53.85	3.79	12.94	6.9618
0 wt%	54.13	9.89	4.313	1.022
1 wt%	54.77	10.06	4.224	0.988
5 wt%	55.33	10.91	3.780	0.840
7.5 wt%	56.99	11.78	2.133	0.720
10 wt%	57.67	12.52	1.997	0.637
14 wt%	58.92	13.88	1.487	0.519
15 wt%	56.71	12.59	1.812	0.630

Fig. 1 XRD spectra of PVA–PVP:(15 − x)CuO(x)MWCNTs PNCs

materials. The results are shown as relative intensities (I/I_0), where I refer to the intensity in counts at any peaks, whereas I_0 signpost intensity of the notable crystalline peak. The existence of intrinsic filler ions throughout the crystalline state interstitial locations of the PVA–PVP backbone may alternatively be viewed as a PVA main chain with the nanofillers [21]. The maximum crystallinity is seen when 'x' represents the filler weight concentration and is equal to 14%. Recrystallisation may also play a role in the surprising variance in defect characteristics of the nanocomposites. Because of these characteristics, the structural regularities of the PVA–PVP host molecule alter with the loading of MWCNTs and CuO nanofillers [14]. Hence, these variables result in enhancing the crystallinity of PVA–PVP blended nanocomposites.

3.2 Atomic Force Microscopy (AFM)

The AFM analysis in tapping mode is to analyse the surface shape and roughness of the prepared composites. Figure 2a and b show AFM pictures of nanocomposite for pure and optimum filler level x = 10 wt% in two-dimensional (2D) views. Using the AFM topography, the root-medium-square (RMS) surface roughness of the composites are assessed in the scan area specified in Table 2. RMS surface ruggedness measures are 1.3nm, correspondingly for x = 14 wt% nanocomposites. The addition of nanofiller MWCNTs and CuO into the PVA/PVP blend enhances the roughness of the RMS varies considerably upto x = 14 wt% filler level. Enhancement in the roughness of the RMS signpost the increase in the crystalline characteristics of nanocomposites. AFM
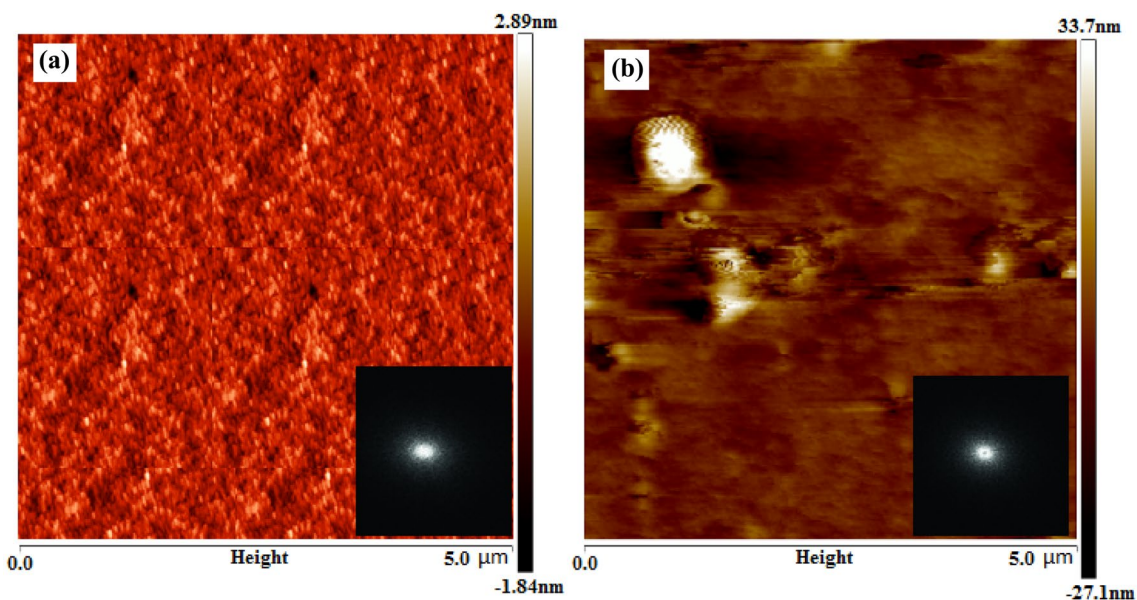

Fig. 2 AFM 2-Dimension photographs with FFT transforms spatial information of **a** Pure PVA and **b** PVA/PVP filled MWCNTs and CuO nanofillers for x = 14 wt% filler concentration

photos also show the rapid two-dimensional Fourier (FFT) transformation of the related pictures. This 2D FFT transforms spatial information into the frequency domain, which is extremely useful for understanding the morphology of the nanocomposite surface. The white dots are the periodicity of surface morphology in the FFT pictures [22]. It is evident that for x = 14 wt% filler level, the white point density is greater than in the pure PVA//PVP blend film. We may thus infer that MWCNTs and CuO nanofillers are randomly orientated into the PVA/PVP matrix that provides a big spot of dispersed intensity at the centre. Figure 3 signifies the 3-D photographs of PVA–PVP:(15-x)CuO(x)MWCNTs for x = 14 wt% nanofiller concentration. AFM measurements acquired particle height ranging upto 33.7nm and also mean particular diameter of approximately 118.43nm within the PVA/PVP matrix.

3.3 Scanning Electron Microscopy (SEM)

Figure 4 refers to SEM surface morphology, indicating that the CuO and MWCNTs are evenly distributed in PVA–PVP mixtures of optimum loading level 14 wt%. Figure 4 also shows that the PVA–PVP mixture has a strong relationship
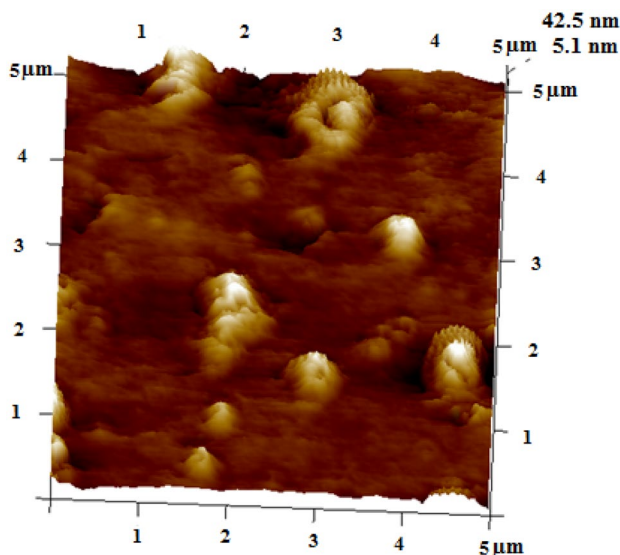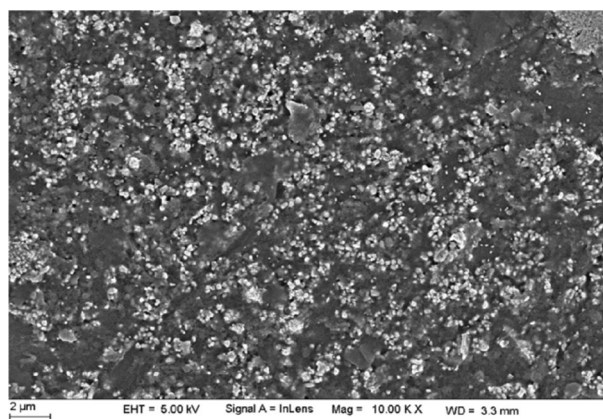

Fig. 4 SEM photographs of PVA–PVP:(15-x)CuO(x)MWCNTs for x = 14 wt%

with CuO and MWCNTs nanofillers forming a homogenous nanocomposite film. The binding among the MWCNTs and CuO nanofillers increases with a reasonably optimum concentration x = 14 wt%. The high concentration of only MWCNTs or CuO nanofillers limits (x = 15wt% or x = 0 wt%) improvement of the structural behaviour of the nanocomposites.

3.4 FTIR Spectral Analysis

Figure 5 continuum obtained revealed typical bending as well as stretching vibration of a structural class of fabricated PVA/PVP:(15-x)CuO(x) MWCNTs PNCs. In a pure PVP/PVA blend, the O–H straining oscillation indicates the existence of the O–H hydroxyl group and is ascribed by the wide and extreme range peaks seen regularly at 2857–3631 cm^{-1}. For the treated PVA/PVP blend, the shifting of the O–H band is observed correspondingly with the rise in nanofiller levels. The surge in filler level upto x = 14 wt% shifts the OH stretching frequencies to the lower wavenumbers than pure PVA/PVP blends. The interaction of CuO and MWCNTs nanofillers with PVA/PVP-OH group is responsible for nanocomposites' structural, optical and electronic properties. The narrowing of the hydroxyl band with the rise in nanofillers signposts the semicrystalline nature of the nanocomposite material. The band at 3577 cm^{-1}, the leading OH vibrational bands of alcohol and phenols, were moved to

Fig. 3 AFM 3-Dimension photograph of PVA–PVP (15-x)CuO(x) MWCNTs for x = 14 wt%

Table 2 AFM parameters of PVA–PVP:(15-x)CuO (x) MWCNTs of optimum filler loading x = 14 wt%

Parameter	Mean	Minimum	Maximum	Sigma
Total Count	8.000	8.000	8.000	0.000
Density	0.320 (/μm²)	0.320 (/μm²)	0.320 (/μm²)	0.000 (/μm²)
Height	14.508 (nm)	5.172 (nm)	42.576 (nm)	14.187 (nm)
Area	58031.082 (nm²)	9536.743 (nm²)	321960.438 (nm²)	100274.750 (nm²)
Diameter	216.134 (nm)	110.193 (nm)	640.260 (nm)	164.844 (nm)

Fig. 5 FTIR spectra of PVP/PVA(15-x)CuO(x) MWCNTs PNCs

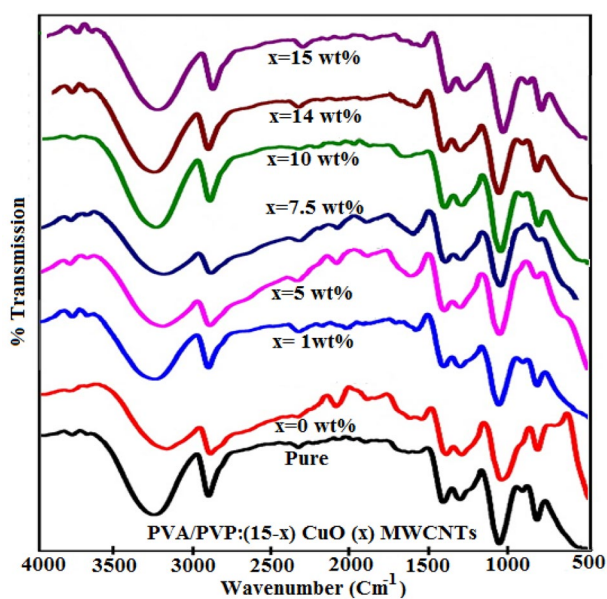**Fig. 6** UV visible spectra of PVA–PVP:(15-x)CuO(x)MWCNTs PNCs

higher wavenumbers with the rise in nanofillers. The addition of nanofiller upto x = 14 wt% resulted in a narrowing of hydroxyl band compared to pure PVA/PVP blend. The peaks recognised at 2570 cm^{-1} seems to be a typical band of oscillations of C–C of the blend. The three bands at 2492, 2320, and 2141 cm^{-1} represent the primary chain PVA/PVP spectra: C–H symmetric distortion, CH_2 deformation, and C=O stretching interacting with loaded nanofillers [23]. The added nanofillers CuO and MWCNTs shift some bands towards the lower frequency range in the FTIR spectra. These alterations indicate how all the C–H compounds in the PVA/PVP connected with added nanofillers resulting in complex conformations [24]. An active absorption band related to symmetric and asymmetric stretching C=O of PVA/PVP blend backbone structure is witnessed at 1714–1011 cm^{-1}. The absorption peaks detected at 918 cm^{-1} represents the syndiotactic structure of PVA/PVP blend. The increase in nanofiller loading enhances the syndiotacticity of PVA/PVP blend, causing dense molecular packing and stronger intermolecular hydrogen bonds. This is responsible for the disappearance of molecular motion resulting in a rise in crystallinity inside the polymer matrix. Thus, the local surface chemistry, internal structural ordering of nanofillers and strain induced by nanofillers with PVA/PVP host matrix resulted in crystalline parameters of PVP/PVA(15-x)CuO(x) MWCNTs PNCs.

3.5 UV Visible Spectroscopic Studies

In work conducted to measure the optical properties of PVA–PVP (15-x)CuO(x) MWCNTs, ultraviolet-visible
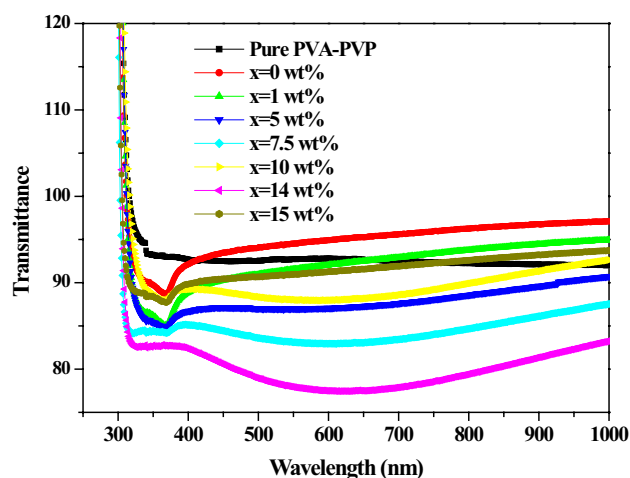
spectroscopic results were used. Figure 6 exemplifies the UV-visible spectra of PNCs for several loading levels. The optical absorption coefficient enhances with a higher loading dosage of MWCNTs and CuO nanofillers. The absorption bands' intensity rises with nanofiller concentration and shows redshifts, suggesting an improvement in charge delocalisation inside the PVA–PVP network. The PVA–PVP primary chain complex interaction with the nanofillers promotes the shift in the absorption band. These complex hydrophobic interactions create more entanglement of nanofillers (complex conformation) with the host matrix, leading to crystalline parameters [25]. The formation of complex conformation found maximum till the filling level reaches x = 14wt %, thereby changing the wavelength of the absorption peaks leading to maximum absorption intensity. Figure 7 confirms an indirect allowed transition of PVA–PVP:(15-x) CuO(x)MWCNTs PNCs provided by the linear behaviour at ambient temperature. An extension of the linear part of the displayed curve from a measure of optical energy band gap E_g of the PVA–PVP: (15-x)CuO (x) MWCNTs to $(ahv)^{0.5} = 0$ produces the outcome of optical energy band gap E_g of PNCs [26, 27]. This graph shows the change in the bandgap of PVA–PVP/ (15-x)CuO(x) MWCNTs concerning x = 0, 1, 5, 7.5, 10, 14, and 15%, respectively. The diminution in the band gap value 2.31 eV with the rise in filler loading for x = 14 wt% is due to occupying nanofillers in the interstitial positions between PVA–PVP chains and promoting complex conformations. The low optical energy gap is 2.31 eV is due to addition of nanofillers which creates the conducting network within the in the PVA/PVP matrix. The low optical energy gap materials are used in solar panels in optoelectronic industry and electronic circuits etc. These results in a charge exchange process between the nanofillers and PVA–PVP chain network, causing the reduction energy gap
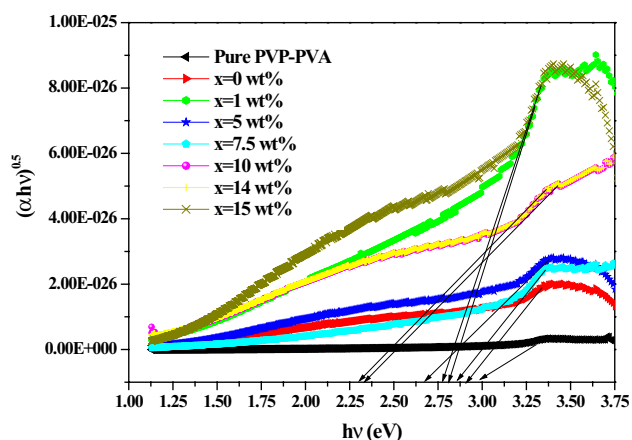
Fig. 7 Variation in energy gap (E_g) of PVA–PVP:(15-x)CuO(x) MWCNTs PNCs

Table 3 DC conductivity parameters of PVA–PVP:(15-x)CuO(x) MWCNTs PNCs

Sl No	Filler Concentration (wt%)	Resistance(?)	Conductivity (s in S/cm)
1	Pure PVA–PVP	10.534×10^6	1.423×10^{-11}
2	0	9.337×10^6	1.605×10^{-11}
3	1	8.134×10^5	1.841×10^{-10}
4	5	7.970×10^5	1.882×10^{-10}
5	7.5	6.334×10^4	2.368×10^{-9}
6	10	2.943×10^4	5.096×10^{-9}
7	14	1.123×10^4	13.35×10^{-9}
8	15	2.278×10^4	6.584×10^{-9}

enhancing the conductivity in the PVA–PVP/ (15-x) CuO(x) MWCNTs nanocomposites.

3.6 DC Conductivity Studies

Table 3 explicit the DC electrical conductivity values of MWCNTs along with CuO nanofillers (x = 0, 1, 5, 7.5, 10, 14 and 15 wt%) in the PVA–PVP matrix. The DC conductivity of PNCs increases by 13.35×10^{-9} S/cm for loading level x = 14 wt%. The MWCNTs and CuO nanofillers inside the PVA–PVP chain network promote charge transfer complexes (CTCs) within the nanocomposites. The semicrystalline PVA–PVP nanocomposites that produce CTCs lead to reduced barrier height and, therefore, allow for better conductivity in the amorphous portions of the polymer matrix [28]. The network of PVA–PVP involves a transport mechanism that comprises rapid intrachain wavelike movement produced by the (bi)polaron wave function overlay on the same PVA–PVP chain. This fallout in leaping activity from site to site is initiated by (bi)polaron's interactions with

neighbouring chains[29]. The filling of nanofillers creates fluctuations in carrier activity, and mobility may result in lower activation energy. It can be reasonably assumed that MWCNTs and CuO nanofillers are distributed throughout the amorphous phase and occupy interstitial locations among PVA–PVP chains. These added nanofillers connect with the PVA/PVP chain via hydrogen bonds by conducting charge among the nanofillers and the PVAPVP network. CTCs enhance the interfacial barrier and reduce the insulator chain transition probability by decreasing the crystalline–amorphous interface. The percolation hypothesis explains how the nanoparticles can form a conducting route between two charging nodes.

In contrast to the carriage of transporters in neutral conjugated polymers, it is necessary to examine the impact of counter ions. The (bi)polarons are isolated traps produced via coulomb interaction of counterions for the small loading level. The increase in the loading level from x = 0 to 14% lowers coulomb traps and enables intra- and inter-chain mobility to the carriers. For the x = 14wt percent optimal filling, these traps overlap by lowering the barrier and promoting movement. Above x> 14 wt%, the carrier's transportation interchain is significantly influenced by morphology and microstructure circumstances that decrease nanocomposites' conductivity [30].

3.7 Thermogravimetric Analysis (TGA)

TGA is an excellent technique for assessing nanocomposite materials' mass changes, heat resistance and thermal decomposition. Figure 8 explores the thermal properties of essential PVP/PVA mix and PNCs PVP/PVA(15-x)CuO(x) MWCNTs with load levels x = 0,1,5,7.5,10,14 and 15wt. A significant weight loss between 120 and 255 °C results in the breakdown of macromolecular chains into tiny fragments [31]. An observed dramatic weight loss over 260 °C is attributable to the thermal decomposition of the PVA/PVP main chains. In most of the tests, a peak between 550 and 650 °C was found ascribed to carbonisation and deterioration of the mixture of polymers [32]. The improvement in thermal stability additionally occurs by changing the curves to greater temperatures by raising the loading levels of nanofillers. The increase of thermal stability may be attributable to the good thermal characteristics of added nanofillers, which encourages the heat dissipation in PVA/PVP matrices [33]. The interfacial interaction as well as surface modification between the nanofillers and the PVA/PVP mixture for optimum filler level x = 14 wt% may further encourage heat dissipation and effectively postpone the breakdown nanocomposites. The strengthening of the interface contact between MWCNTs with CuO nanofillers and PVA/ PVP PNCs dispersion upto x = 14 wt% loading level may
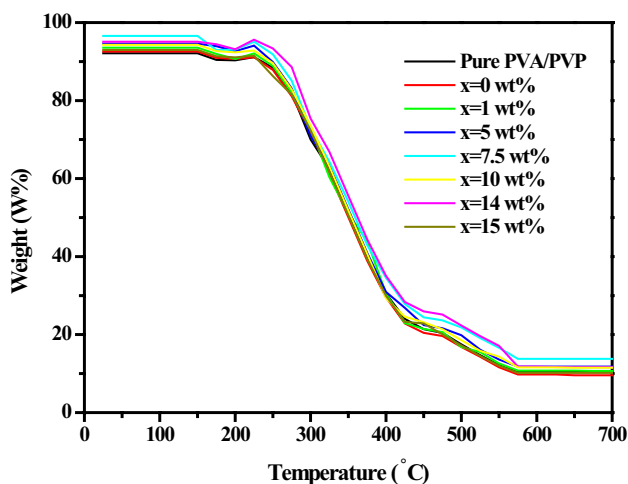
Fig. 8 TGA thermograms of PVP/PVA(15-x)CuO(x) MWCNTs PNCs for various filler concentrations

Table 4 Activation energy and percentage crystallinity of unfilled and filled PNCs employing Coats-Redfern and Broido techniques

Nanofiller loading Concentration 'x' (wt%)	Coats - Redfern method (KJ/mol)	Broido method (KJ/mol)	Percentage Crystallinity
Pure PVA/PVP	260.2	257.5	50.77
0	258.3	254.9	52.84
1	254.7	250.1	53.17
5	250.7	246.7	54.11
7.5	243.8	238.4	54.78
10	236.3	231.8	55.11
14	227.6	222.7	56.34
15	237.1	234.2	55.01

perhaps lead to the better thermal stability matched with pure PVA/PVP blend.

3.7.1 Calculation of the Activation Energy

To calculate the thermodynamics parameters obtained from the TGA curves, the following two methods are employed.

3.7.1.1 Coats–Redfern Method It is an example of an integral method in which activation energy analysis is performed as follows [34]:

$$log\left[\frac{-\log(1-\propto)}{T^2}\right] = log\frac{R}{\Delta E_\propto}\left[1 - \frac{2RT}{E_\propto}\right] - 0.434\frac{E_\propto}{RT} \quad (2)$$

where, R = 8.3136 J/mol K (the universal gas constant), T signposts the absolute temperature, E_a refers to activation energy (J/mol) and a denotes weight loss of conversion fraction.

In tracing the dependency of $log\left[\frac{-\log(1-\propto)}{T^2}\right]$ versus $\frac{1000}{T}$ related to the individual specimen, a straight line has been achieved and considering the paths, the activation energy may be computed as:

$$E_\alpha = Slope \times 2.303R \quad (3)$$

3.7.1.2 Broido Method Broido introduces a methodology to determine activation energy during phase two of breakdown employing the formula:

$$\ln\left[\ln\left(\frac{1}{Y}\right)\right] = \left(\frac{E_\alpha}{R}\right)\frac{1}{T} + constant \quad (4)$$

In the above expression, 'Y' gives the number of undecomposed initial molecules and are estimated employing the equation:

$$Y = \frac{W_t - W_\infty}{W_i - W_\infty} \quad (5)$$

where W_t, W_∞, Wi represents the weight, weight zero and first weight at any time t, respectively. A graph of ln [ln (1/Y)] vs. 1/T provides excellent proximity to a straight path. Considering consecutive lines, we computed slope, which gives the activation energy [35]. Table 4 explores the activation energy (E_a) measurements in Coats – Redfern and Broido technique that diminish the upsurge value in nanofillers loading level upto x = 14 wt%. This shows that the PVA/PVP mix is intensely affected by the presence of nanofillers in its main chain.

The observation in Table 4 suggests that both the models exhibit fairly the good value of activation energy of the prepared nanocomposites. However, the occurrence of many homogeneous and heterogeneous pathways during thermal decomposition phenomenon of nanocomposites is much exhibited by Coats-Redfern technique. Hence, small difference is witnessed in activation energy as well as percentage crystallinity of the unfilled and filled PNCs.

3.8 Photoluminescence

Figure 15 signposts the photoluminescence of PVP/PVA(15-x)CuO(x) MWCNTs PNCs with a percentage loading levels for x = 0, 1, 5, 7.5, 10, 14 and 15 wt, employing fluorescence spectrophotometer-Cary Eclipse. PL is an operational method that estimates electronic structure affected by the complex particle dimension formed due to crystallinity. The PL analyses for produced PNCs were conducted on a surge wavelength of 375nm at room temperature. The PNCs exhibit exciting pinnacles at 380nm and precise, strong emission bands within 650nm visible range by disregarding a

specific harmonic reflection order [36]. The initial strong PL in the near UV–vis regions represents the planar PVA/PVP polymer molecules. The wide emission spectrum found for PVA/PVP nanocomposite correlates to the electronic shift of the OH side-chain typical of the three different aqueous, isotactic, syndiotactic and atactic polymer configurations [37]. A prominent emission band at 638 nm resembles the electron-hole recombination of MWCNTs and CuO nano-fillers. The broadband emission of the PL of PVP/PVA(15-x)CuO(x)MWCNTs nanocomposites is attributed by some authors are due to CuO structural defects (green areas), as oxygen vacancies, and MWCNTs, as well as certain impurities (yellow and orange areas) [38] (Fig. 9).

3.9 Dielectric Studies

Figures 10, 11 and 12 signifies the spectra of complex dielectric permittivity (real part ϵ' and imaginary part ϵ'') and the dielectric loss tangent (tan d) of PVA–PVP/(15–x) CuO (x) MWCNTs composites for various concentrations at room temperature. Figure 10 explores the PNCs ϵ' values are decreasing with an applied frequency rise [39]. Figure 10 also shows the decrement in ϵ' values of unclassified PVA– PVP blend mix in the non-linear range from 14.62 to 6.32 with the rise in applied frequency from 1 kHz to 1 MHz, whereas for PNCs, the ϵ' values decreased almost linearly in the range 26.97–2.81, suggesting the tunable frequency behaviour. The substantial reduction of ϵ' values across the lower frequency range of x = 14 wt% filler level are evidence of the significant impact of the nano-confinement effect in the PVA/PVP network. It is well known that the nano-confinement impact is primarily an increased impediment of dipolar units in the PVA–PVP network created by the nanofillers with a time-different electric field, which decreases the dipolar polarisation of the PVP/PVA(15-x)CuO(x) MWCNTs PNCs [40]. The increment in frequency
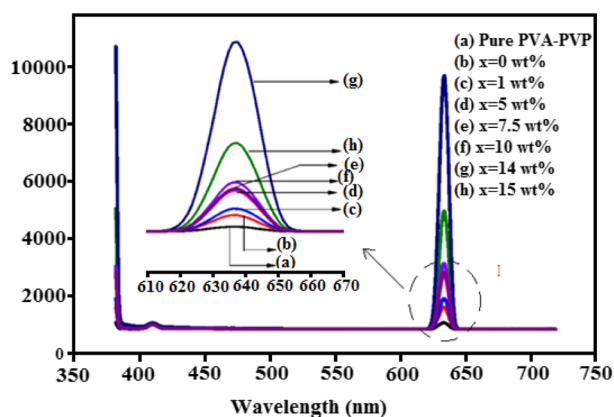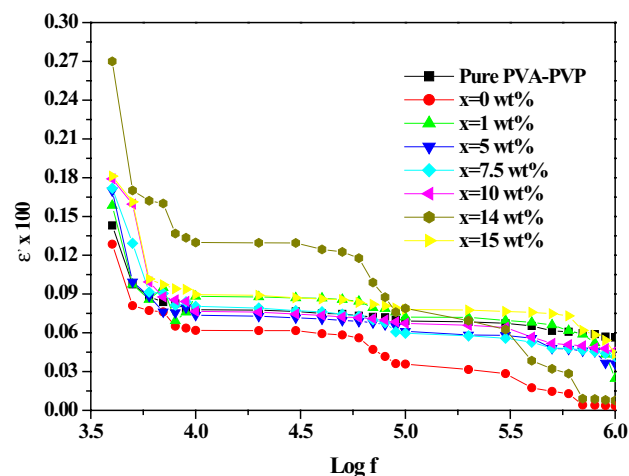
Fig. 10 Deviation of real dielectric constant of PVA/PVP:(15-x) CuO(x)MWCNTs PNCs for different filler concentration

towards a higher frequency range indicates that the values of ϵ' for PVP/PVA(15-x)CuO(x) MWCNTs PNCs for x = 14 wt% are comparable to those of the other filler loading nanocomposites, which suggests that the nanocontainment effect plays no role in the higher frequency dielectric polarisation. The ϵ' and Tan d values in Figs. 11 and 12 decreased substantially at low frequencies and showed a reasonably steady behaviour compared to unfilled PVA–PVP mix film. The result shows that x = 14 wt% nanofiller loading significantly decreases low-frequency dielectric losses in the PVA–PVP mix. Furthermore, there has been a substantial reduction in the ϵ' values of PNC films with a further rise in loading level upto x = 14 wt%. The ϵ' and Tan d values initially decreased slightly with the rise in frequency and slightly increased trend for higher applied frequencies

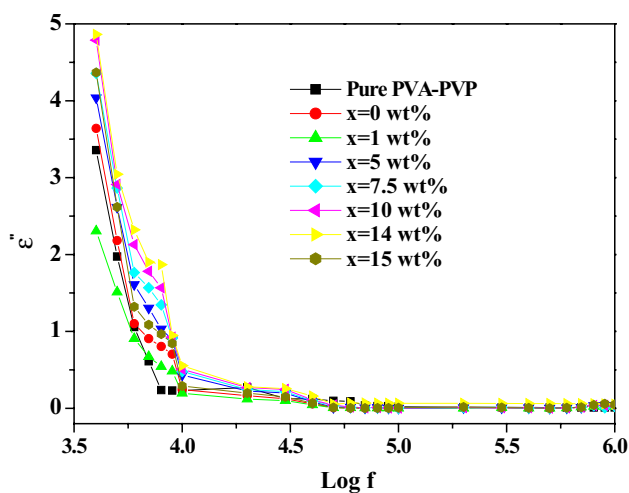**Fig. 9** PL spectra of pure PVA/PVP and filled PNCs with excitation wavelength 375nm

Fig. 11 Variation of imaginary dielectric constant for different filler levels of PVA–PVP:(15-x)CuO(x)MWCNTs PNCs
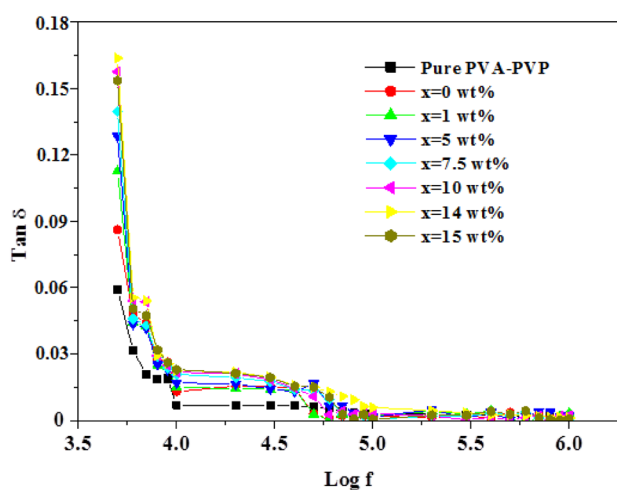
Fig. 12 Variation of dielectric loss for different filler levels of PVA–PVP:(15-x)CuO(x)MWCNTs PNCs

(i.e. f > 10 kHz). For x = 14 wt% loading level, the ϵ' and Tan d spectra of PVP/PVA(15-x)CuO(x) MWCNTs nanocomposites exhibit decreasing trends between 1 kHz and 10 kHz. At the same time, the observational frequency range between 10 kHz and 1 MHz dielectric relaxation reduces, contributing to the conductivity [41]. Thus, ϵ' and Tan d these PNCs upto x = 14 wt% show a gradual improvement in the parameter values with an increase in frequency and at higher applied frequency shows a dipolar relaxation process in these materials.

4 Conclusions

In this current research, the effects of structural, optical, thermal, dielectric and electrical properties of copper dioxide (CuO) nanoparticles and multiwall carbon nanotubes (MWCNTs) filled PVA and PVP blend matrix (50/50 wt%) established polymer nanocomposites (PNCs) (i.e., PVA/PVP:(15-x)CuO(x)MWCNTs for x = 0,1,5,7.5, 10,14, and 15wt%) are reported. X-ray diffraction investigation reports the increase in crystallinity of PNCs for x = 14 wt% filler level. The FTIR, SEM, and AFM measurements of PVA/PVP:(15-x)CuO (x)MWCNTs for x = 0,1,5,7.5, 10,14, and 15wt% provides the information of miscible mix, PVA–PVP interaction and polymer–nanoparticle interfaces, and the influence of CuO and MWCNTs nanofillers on the morphology aspects on the network of PVA/PVP blend. Optical studies shows the nanofiller dispersion for x = 14 wt% nanoloading in the PNCs matrix considerably enhances the crystalline phase, diminishing its optical energy gap to 2.31 eV. The DC conductivity values enhance to 13.35×10^{-9} S/cm with the upsurge in optimum filler level x = 14 wt%. The photoluminescence studies of PNCs exhibit exciting pinnacles

at 380nm and precise, strong emission bands within 650nm visible range by disregarding a specific harmonic order of reflection. TGA studies show that strengthening the interface contact between MWCNTs with CuO nanofillers and PVA/PVP PNCs dispersion upto x = 14 wt% loading level may improve thermal stability matched with pure PVA/PVP blend. The dielectric and electrical characteristics of these PNCs are investigated for an applied frequency range from 1 kHz to 1 MHz. The enhancement in the nanofiller level upto x = 14 wt% in the PNCs matrix leads to the development of percolating network through the PNCs. These factors boost the dielectric permittivity values substantially, owing to the decrease in the nano-confinement phenomenon. The rise in applied frequency reduces the real portions of dielectric permittivity and enhances electrical conductivity. These PVA / PVP :(15-x)CuO (x)MWCNTs having good dielectric and electrical characteristics can be used as frequency tunable dielectric PNCs in electronic devices.

Declarations

Conflict of interest The author declares no conflict of interest.

References

1. M.M. Demir, M. Memesa, P. Castignolles, G. Wegner, PMMA/zinc oxide nanocomposites prepared by in-situ bulk polymerization. Macromol. Rapid Commun. **27**(10), 763–770 (2006)
2. E.M. Abdelrazek, I.S. Elashmawi, A. El-Khodary, A. Yassin, Structural, optical, thermal and electrical studies on PVA/PVP blends filled with lithium bromide. Curr. Appl. Phys. **10**, 607–613 (2010)
3. M. Todd Alam, J.U. Otaigbe, D. Rhoades, G.P. Holland, B.R. Cherry, P.G. Kotula, Nanostructured polymer blends: synthesis and structure. Polymer **46**(26), 12468–12479 (2005)
4. R. Baskaran, S. Selvasekarapandian, N. Kuwata, J. Kawamura, T. Hattori, Conductivity and thermal studies of blend polymer electrolytes based on PVAc–PMMA. Solid State Ionics **177**, 2679–2682 (2006)
5. K.K. Kumar, M. Ravi, Y. Pavani, S. Bhavani, A.K. Sharma, V.V.R. Narasimha Rao, Investigations on PEO/PVP/NaBr complexed polymer blend electrolytes for electrochemical cell applications. J. Membr. Sci. **454**, 200–211 (2014)
6. N.B. Rithin Kumar, S. Acharya, A. Alhadhrami, B.M. Prasanna, S.C. Gurumurthy, Role of TiO2/ZnO nanofillers in modifying the properties PMMA nanocomposites for optical device applications. Iran. J. Sci. Technol. Trans. Sci. (2021). https://doi.org/10.1007/s40995-021-01183-4
7. K. Phiwdang, S. Suphankij, W. Mekprasart, W. Pecharapa, Synthesis of CuO nanoparticles by precipitation method using different precursors. Energy Proc. **34**, 740–745 (2013)
8. N. Rajeswari, S. Selvasekarapandian, C. Sanjeeviraja, J. Kawamura, S. Asath Bahadur, A study on polymer blend electrolyte based on PVA/PVP with proton salt. Polym. Bull. **71**, 1061–1080 (2014)

9. C.V. Subba Reddy, A.K. Sharma, V.V.R. Narasimha Rao, Electrical and optical properties of a polyblend electrolyte. Polymer **47**, 1318–1323 (2006)

10. Z.D. Dai, L. Ansaloni, D.L. Gin, R.D. Noble, L.Y. Deng, J. Membr. Sci. **523**, 551–560 (2017)

11. B. Yalagala, S. Khandelwal, J. Deepika, S. Badhulika, Wirelessly destructible MgO-PVP-graphene composite based flexible transient memristor for security applications. Mater. Sci. Semicond. Process. **104**, 104673 (2019)

12. F.M. Ali, R.M. Kershi, M.A. Sayed, Y.M. AbouDeif, Evaluation of structural and optical properties of Ce3 + ions doped (PVA/PVP) composite films for new organic semiconductors. Physica B Condens. Matter **538**, 160–166 (2018)

13. S. Mahendia, G. Kandhol, U.P. Deshpande, S. Kumar, Determination of glass transition temperature of reduced graphene oxide-poly(vinyl alcohol) composites using temperature-dependent Fourier transform infrared spectroscopy. J. Mol. Struct. **1111**, 46–54 (2016)

14. R.F. Bhajantri, V. Ravindrachary, B. Poojary, A. Harisha, V. Crasta, Studies on fluorescent PVA + PVP + MPDMAPP composite films. Polym. Eng. Sci. **49**(5), 903–909 (2009)

15. A. Azam, A.S. Ahmed, M. Oves, M.S. Khan, A. Memic, Size-dependent antimicrobial properties of CuO nanoparticles against gram-positive and -negative bacterial strains. Int. J. Nanomed. **7**, 3527–3535 (2012)

16. X. Peng, S.S. Wong, Functional Covalent Chemistry of Carbon Nanotube Surfaces. Adv. Mater. **21**(6), 625–642 (2009). https://doi.org/10.1002/adma.200801464

17. R. Jeyaraman, J. Kadarkaraithangam, M. Arumugam, R. Govindasamy, A. Abdul.Synthesis and antimicrobial activity of copper nanoparticles. Mater. Lett. **71**, 114–116 (2011)

18. Z. Liu, L. Jiao, Y. Yao, X. Xian, J. Zhang, Aligned, ultralong single-walled carbon nanotubes: from synthesis, sorting, to electronic devices. Adv. Mater. **22**(21), 2285–2310 (2010). https://doi.org/10.1002/adma.200904167

19. S.H. Park, W.J. Lee, Hierarchically mesoporous CuO/carbon nanofiber coaxial shell-core nanowires for lithium ion batteries. Sci. Rep. **5**, 9754 (2015)

20. M. Sahooli, S. Sabbaghi, R. Saboori, Synthesis and characterization of mono sized CuO nanoparticles. Mater. Lett. **81**, 169–172 (2012)

21. H.M. Zidan, J. Appl. Polym. Sci. **88**, 1115–1120 (2003)

22. N.B. Rithin Kumar, B.M. Vincent Crasta, Enhancement of optical, mechanical and micro structural properties in nanocomposite films of PVA doped with WO3 nanoparticles. Int. J. Struct. Integr. **6**(3), 338–354 (2015)

23. G.N. Hemanth Kumar, J. Lakshmana Rao, N.O. Gopal, K.V.C. Narasimhulu, R.P.S. Chakradhar, A. Varada Rajulu, Spectroscopic investigation Mn+2 ions doped polyvinyl alcohol films. Polymer **45**, 5407–5415 (2004)

24. E.M. Abdelrazek, A.M. Abdelghany, A.H. Oraby, G.M. Asnag, Investigation of mixed filler effect on optical and structural properties of PEMA films. Int. J. Eng. Technol. **12**, 98–102 (2012)

25. I. Saini, J. Rozra, N. Chandak, S. Aggarwal, P.K. Sharma, A. Sharma, Tailoring of electrical, optical and structural properties of PVA by adding Ag nanoparticles. Mater. Chem. Phys. **139**, 802–810 (2013)

26. E.A. Davis, N.F. Mott, Conduction in non-crystalline systems. V. Conductivity, optical absorption and photoconductivity in amorphous semiconductors. Philos. Mag. **22**, 0903–0922 (1970)

27. N.F. Mott, Conduction in non-crystalline systems: IV. Anderson localization in a disordered lattice. Philos. Mag. **22**, 7–29 (1970)

28. B.A. Collins, J.E. Cochran, H. Yan, E. Gann, C. Hub, R. Fink, C. Wang, T. Schuettfort, C.R. McNeill, M.L. Chabinyc, H. Ade, Polarized X-ray scattering reveals non-crystalline orientational ordering in organic films. Nat. Mater. **11**, 536–543 (2012)

29. R. Noriega, J. Rivnay, K. Vandewal, F.P. Koch, N. Stingelin, P. Smith, M.F. Toney, A. Salleo, A general relationship between disorder, aggregation and charge transport in conjugated polymers. Nat. Mater. **12**, 1038–1044 (2013)

30. S.D. Kang, G.J. Snyder, Charge-transport model for conducting polymers. Nat. Mater. **16**, 252–257 (2017)

31. S.N. Patel, A.M. Glaudell, K.A. Peterson, E.M. Thomas, K.A. O'Hara, E. Lim, M.L. Chabinyc, Morphology controls the thermoelectric power factor of a doped semiconducting polymer. Sci. Adv. **3**, e1700434 (2017)

32. H.-S. Kim, H.-S. Yang, H.-J. Kim, H.-J. Park, J. Therm. Anal. Calorim. **76**, 395–404 (2004)

33. G. Zuo, X. Liu, M. Fahlman, M. Kemerink, High seebeck coefficient in mixtures of conjugated polymers. Adv. Funct. Mater. **28**, 1703280 (2018)

34. A.W. Coats, J.P. Redfern, Nature **201**, 68–69 (1964)

35. A. Broido, J. Polym. Sci. A **2**(7), 1761–1773 (1969)

36. B.G. Shetty, N.B.V. Crasta, R. Kumar, K. Rajesh, R. Bairy, P.S. Patil, Promising PVA/TiO2, CuO filled nanocomposites for electrical and third order nonlinear optical applications. Opt. Mater. **95**, 109218 (2019)

37. E.S. Mora, E.G. Barojas, E.R. Rojas, R.S. Gonzalez, Sol. Energy Mater. Sol. Cells **91**, 1412–1415 (2007)

38. M. Mazzera, M. Zha, D. Calestani, A. Zappettini, L. Lazzarini, G. Salviati, L. Zanotti, Nanotechnology **18**, 355707 (2007)

39. N.B. Rithin Kumar, V. Crasta, B.M. Praveen, Dielectric and electric conductivity studies of PVA (Mowiol 10-98) doped with MWCNTs and WO3 nanocomposites films. Mater. Res. Express **3**(5), 055012 (2016)

40. D. Mardare, G.I. Rusu, Ccomparison of the dielectric properties for doped and undoped TiO2 thin films. J. Optoelectron. Adv. Mater. **6**, 333–336 (2004)

41. V. Rao, P.V. Ashokan, M.H. Shridhar, Studies of dielectric relaxation and a.c. conductivity in cellulose acetate hydrogen phthalate-poly (methyl methacrylate) blends. Mater. Sci. Eng., A **281**, 213–220 (2000)

Publisher's Note Springer Nature remains neutral with regard to jurisdictional claims in published maps and institutional affiliations.